Flash boiling in a multihole G-DI injector – Effects of the fuel distillation curve

Lucio Araneo [a, b], Roberto Donde' [a, *]

[a] CNR-ICMATE, via Cozzi 53, 20125 Milano, Italy
[b] Politecnico di Milano, Dipartimento di Energia, via Lambruschini 4A, 20156 Milano, Italy

The effects of fuel temperature and chamber pressure on the spray of a multi-hole G-DI injector were analyzed in a qui-escent test chamber. The analysis was focused on the behavior of the global spray angles both close and far from the injector. Three pure hydrocarbons (*n*-hexane, *n*-heptane, and isooctane), three gasolines of known distillation curve and a commercial 95 RON gasoline from a gas station were utilized. The tests were performed at four chamber pressures (atmospheric, 80 kPa, 60 kPa and 40 kPa) and the fuel temperature was varied from 30 °C to 110 °C.

The results for *n*-hexane and gasolines were very similar, while *n*-heptane and isooctane showed a different behavior.
The ratio between the fuel saturation pressure at the operating temperature and the air pressure (p_S/p_a) is confirmed as a fundamental parameter for spray angle data reduction. The near field spray angle data for pure hydrocarbon fuels merge to a unique curve when plotted in function of p_S/p_a. An approximated method to deduce the gasoline saturation pressure curves starting from the distillation curve is presented. Using the calculated saturation pressures for the reduction of near field spray angle data for the gasolines, a unique curve is obtained, coincident with that of the tested pure hydrocarbons. In alternative, from the results obtained for a fuel of known saturation pressure curve, it is possible to obtain a direct cor-relation between near field spray angle and saturation pressure. From this relationship, an approximated saturation pres-sure curve from the experimental angle measurements obtained on the same injector for an unknown fuel can be derived.

Keywords: Flash boiling, Direct injection spark ignition, Spray angle, Gasoline, Distillation curve

Nomenclature

c_p	specific heat
p_a	air pressure
p_s	saturation pressure
T_f	fuel temperature
T_s	saturation temperature
ΔH_v	latent heat of evaporation
ρ_l	liquid density
ρ_v	vapor density

Abbreviations

ASOI	After Start Of Injection
ASTM	American Society for Testing and Materials
DIPPR	Design Institute for Physical Properties
G-DI	Gasoline Direct Injection
NIST	National Institute of Standards and Technology
RON	Research Octane Number
SAE	Society of Automotive Engineers
TBP	True Boiling Point

1. Introduction

It is well known that rapid evaporation occurs when a liquid is injected in an ambient at pressure below its saturation pressure. The sensible heat of the fuel provides the latent vaporization heat for a fraction of the liquid mass. After the pioneering work by Brown and York [1], numerous studies on the phenomenon in pools, ducts, jets, films and sprays were published. Although the physical bases are the same, the practical effects of interest in the various configurations could be different. Many studies were focused on transition from Rayleigh jet regime to spray regime by flash boiling. The aim was to obtain a good atomization with low pressure atomizers. An overview of the state of the art on this aspect of flash boiling is given in Sher et al. [2]. Different is the scope of the present work. In this case the effects of the phenomenon on a real G-DI injector at real injection pressure are studied. It means that a fully developed breakup regime is considered even in absence of flash boiling.

As the G-DI technology developed, the behavior of different injector types was reported in literature. From the first studies devoted to swirl injectors [3–9], the attention lately moved to other injector types [10–24], however the studies on swirl injectors were not abandoned [25]. From the experimental results reported in the cited literature, a clear effect of flash boiling both on the spray shape and on the droplet diameters was noticed both for swirl and for multi-hole atomizers. The effects on both types of atomizers are similar. In particular,

Article history:
Received 22 January 2016
Received in revised form 28 September 2016
Accepted 26 November 2016

* Corresponding author.
Email address: roberto.donde@cnr.it (R. Donde')

Published Journal Article available at: http://dx.doi.org/10.1016/j.fuel.2016.11.104

flash boiling causes an increase of the spray angle at the nozzle exit [4,5,9,10,12,13,16,19,24], that is followed by a contraction of the angle as the distance from the nozzle increases [5,10,12–14,18].

It is evident that the choice of the position where the spray angle is measured strongly affects the results, so quantitative comparison of works from different origins with different processing criteria cannot be immediately performed. In some cases, the angle definition gives as a consequence a behavior apparently opposite to the actual one. It would be desirable to define some standard procedures to measure the spray angles in order to obtain a comparable description of the actual spray behavior.

The SAE J2715 [26] Recommended Practice has some limitations when applied to a flashing spray. Depending on the injector design, the recommended measurement range from 5 mm to 15 mm could interest a region where the transition between angle increase and angle decrease occurs.

The spray penetration is affected both by the degree of overheating and by the ambient pressure [12,19,21,24]. The mean droplet size was observed to decrease in presence of flash boiling [4,6,11,14,16,21]. These effects could be either favorable or detrimental depending on the applications, from this fact follows the importance of the studies about this topic. For this reason the authors carried up in the past studies on a G-DI swirl injector using simple fuels [9]. The results, reported in Fig. 1, demonstrated that the angle at the exit of the injector was greatly influenced by flash boiling. Infact as soon as the phenomenon starts to occur the spray angle increases. Testing mixtures of *n*-pentane and isooctane in different percentage at atmospheric pressure, the angle increase starts to occur at higher temperature as the percentage of the higher boiling component (isooctane) is increased (Fig. 1a). Plotting the same results in terms of the ratio between saturation pressure and ambient pressure (p_s/p_a) instead of temperature, the experimental curves merge in a unique curve as shown in Fig. 1b. When the value of p_s/p_a becomes greater than one the spray angle starts to increase and for values greater than 1.5 the data can be fitted by a logarithmic curve. Furthermore, the saturation pressure to be considered resulted to be the average saturation pressure of the mix, with no dominant effects of the lighter element. Considering these previous results, the authors decided to extend the investigation to a new generation multi-hole injector and different distillation gasolines. The examined results regard mainly the effects of flash boiling on the near field global angle of the injector spray. The main scope of the work is the setup of a procedure to study the effect of different distillation curve gasolines on the behavior of the injector spray in flash boiling conditions.

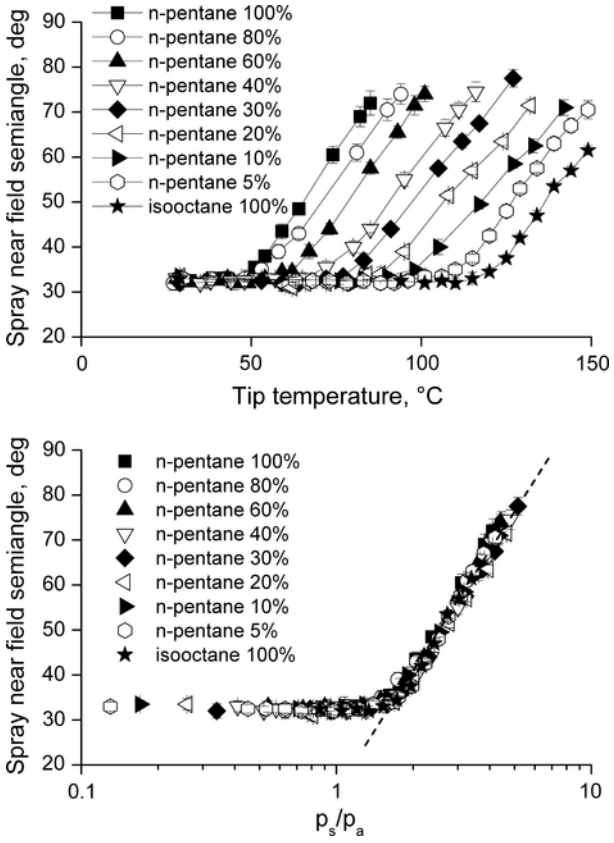

Fig. 1. Swirl injector near field spray semiangle variation with fuel temperature for different *n*-pentane/isooctane mixtures (a) and the same data plotted in terms of normalized pressure (saturation pressure/air pressure) [9].

2. Experimental setup and procedure

A six holes G-DI injector was tested in a constant volume chamber. The spatial distribution of the injector jets at 30 mm distance from the tip is reported in Fig. 2, where the arrow indicates the line of sight of the camera. Four of the six jets are nearly aligned in the visualized image plane, while the other two are aligned along the line of sight.

The nominal value of the spray angle in the image plane is 72° and the nominal single beam angle is 19°. The nominal static mass flow rate is 923.5 g *n*-heptane per minute at 10 MPa injection pressure.

The test chamber has an internal volume of 10 l (206 mm internal diameter and 300 mm height) and has four 90 mm diameter windows positioned at 0°, 110°, 180° and 270° angles for visualizations and optical diagnostics. The chamber walls can be heated by electric cartridges and the input air can be preheated in an electrically heated reservoir. The air temperature inside the chamber is monitored by means of a J type thermocouple whose tip is placed near the injector tip but out of the spray range. In the present study, the chamber air temperature was kept at 25 °C.

For the tests, the chamber pressure was varied from ambient pressure down to 40 kPa absolute pressure using a compressed air ejector. The pressure regulation was obtained acting both on ejector applied air pressure and on input airflow. The airflow was optimized to have a complete evacuation of the injected fuel during the interval between two consecutive injections without influencing the spray behavior.

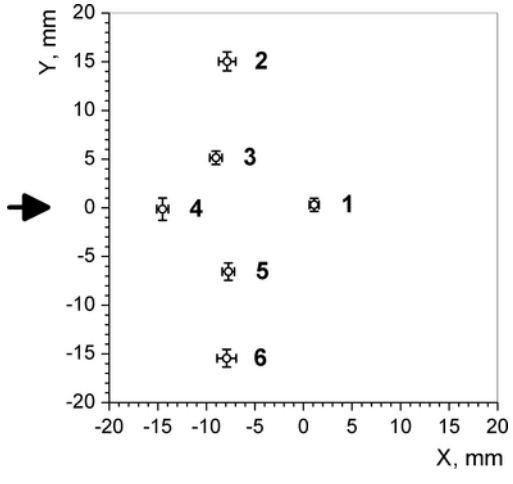

Fig. 2. Spatial distribution of the injector jets at 30 mm distance from the tip.

Moreover, the airflow was effective in avoiding the increase of the chamber air temperature due to the presence of the injector heater.

The fuel was pressurized using a sac pressure accumulator in order to avoid direct contact of the fuel with the pressurizing gas. The fuel was pumped in the circuit by a normal automotive electric pump and, after a period of recirculation in order to purge the circuit from gas bubbles, the gas pressure in the accumulator was reduced below the pump pressure to allow the accumulator filling. After that, the filling circuit was closed and the fuel was pressurized to the wanted injection pressure by supplying nitrogen to the gas section of the accumulator. The pressure was controlled by a pressure transducer and a feedback circuit acting on a solenoid valve. The tests were performed at 10 ± 0.05 MPa fuel injection pressure.

The injector was placed at the center of the upper flange of the chamber using an appositely designed adapter. The injector was surrounded by an oil jacket heated by two electric cartridges placed on the sides. A J-type thermocouple placed in contact with the injector measured the tip temperature and gave the feedback to the electric cartridges PID controller.

The injector nose temperature was varied from 30 to 110 °C with 20 °C steps. The injection duration was set to 3 ms and the repetition rate was limited to 0.5 Hz in order to guarantee that the fuel temperature was as close as possible to that of the injector nose. The low injection frequency also facilitated the test chamber air renewal between the injections. The steadiness of the injection temperature was controlled a posteriori by observing the absence of any particular temporal trend in the results obtained at constant conditions.

Seven different fuels were investigated: three gasoline formulations of known distillation curve, a commercial gasoline (RON 95) from a gas station, *n*-hexane, *n*-heptane and isooctane.

The effects of flash boiling on the spray structure were studied by comparing the images of the spray in different operative conditions.

The imaging setup consisted in a Z-schlieren apparatus [27] without knife, thus allowing backlight imaging and no perspective effects. A stroboscopic flash lamp with a flash duration of about 30 μs was used as light source and the images were taken by a PCO Sensicam camera setting the exposure time at 3 μs. The timings of injector, flash lamp and CCD camera were controlled by a multichannel pulse generator. Particular care was taken in the optical system alignment in order to have a uniform background and a neat contrast with the spray edge. The background quality was used also as a criterion for the airflow setting. The airflow was increased and the repetition rate reduced until the presence of residual fuel fog from the previous injection was negligible. The optical setup was adjusted to have an image spatial resolution of 0.1 mm per pixel. This choice was dictated by the compromise between the necessity of a complete view of the spray far field and the accuracy in near field angle measurement. As a result, the pixel resolution introduces an uncertainty in the near field angle measurement of about 3° on the spray angle at cold conditions, This uncertainty decreases to 1.5° at 60° spray semiangle, 0.6° at 70° and 0.15° at 80° spray semiangle. This uncertainty was found to be within the shot to shot experimental variability.

Series of thirty single shot images at 1, 2 and 3 ms delay ASOI were taken for every experimental condition. Every single image was analyzed to extract the angle data. The results were then averaged and the standard deviation value was calculated.

The global envelope of the spray was considered for the measurement of the spray angles, therefore the angles between the external edges of jet 2 and jet 6 of the spray were measured. In particular, the spray near field angle (from 0 to 1 mm from the nozzle) and far field angles (in the ranges 20–30 mm, 30–40 mm and 40–50 mm from the nozzle) were measured.

The images were automatically analyzed using an “ad hoc” macro running in Image Pro Plus software. The first step of the image analysis consisted in a normalization, based on the intensity value of a region of the image far from the spray, to correct for possible shot-to-shot variation of the light intensity. Than a background subtraction using an image taken before the injector opening was performed. The following steps of the analysis for the near field angle measurement are reported in Fig. 3. The resultant image (a), where the spray appears dark on a bright background, was inverted to have a white spray on a dark background (b). Due to the good contrast given to the images by the optical setup, a sharp transition between the spray image and the background was obtained. After a preliminary sensitivity analysis a threshold of 10% of the range of the intensity profile was chosen to identify the spray edge. The image was then binarized using this threshold (c). The angles were calculated by connecting the points determined by the intersections of the spray profile with two lines normal to the spray axis traced at the beginning and at the end of the defined distance range (d). It is particularly important to choose a very short distance for the near field angle. This because

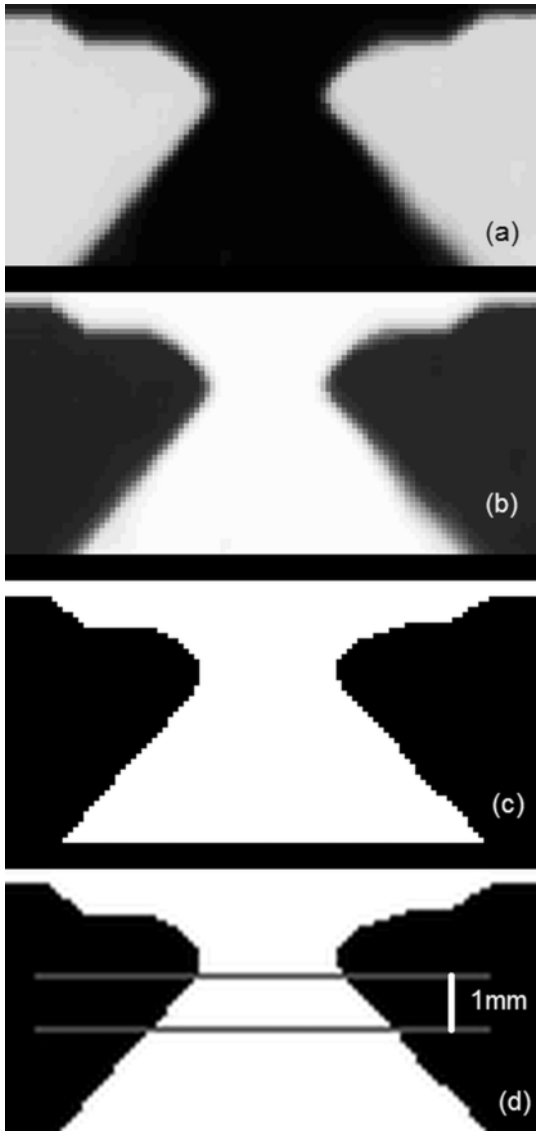

Fig. 3. Image analysis steps for the near field angle measurement.

the dominance of the flash boiling phenomenon in enlarging the spray contour is very short living. At few millimeters from the nozzle the spray profile begins to bend toward the spray axis due to the induced air flow field. An example is shown in Fig. 4 where a binarized image of a highly flashing spray is reported. The reference lines traced at a distance of 1 mm and 5 mm from the injector tip allow to appreciate at a glance how close to the nozzle the induced air flow field begins to dominate the spray shape. This image shows also a limitation in the adopted method as, in these conditions, even in the distance range of 1 mm from the injector tip, the spray edge is not linear. For this reason at 1 mm distance from the nozzle a near field spray angle value lower than the real angle at the nozzle exit is obtained.

A resume of the experimental conditions is given in Table 1.

3. Experimental results

As reported before, the aim of this work was the study of the effects of flash boiling on the spray structure of different fuels. This was obtained by increasing the fuel temperature, at constant air pressure, from 30 °C up to 110 °C and measuring some spray characteristic angles. The procedure was repeated at four different air pressure values (40, 60, 80 kPa and atmospheric pressure) for each one of the seven fuels.

In Fig. 5, two images of the spray both in absence (a) and in presence (b) of flash boiling are compared. Close to the nozzle, the spray angle increases for the effect of flash boiling. After the initial angle widening, the spray side boundary tends to curve toward the axis causing a contraction of the spray width. This spray collapse was observed by many researchers [5,10,12–14,16,18,21,25] both in swirled and in multi-hole injectors. It was explained by the decrease of droplet mean diameter observed when flashing occurs [21,25]. In fact, smaller droplets are more easily driven toward the spray axis by the induced airflow.

In Fig. 6a–d, the average values of the spray semiangle measured at 1 mm distance from the nozzle are reported in function of the fuel temperature for each test chamber pressure value. The error bars shown both in these and in all the following graphs indicate plus-minus one experimental standard deviation around the mean. A clear difference in the behavior of isooctane and *n*-heptane with respect to the other fuels is noticed. For these pure hydrocarbons, at atmospheric pressure (Fig. 6a), the spray angle increase occurs around 100 °C. This is in agreement with their atmospheric boiling points of 99 °C and 97 °C. The *n*-hexane curve indicates that the angle increase occurs at about 70 °C. Even for this fuel the transition temperature is close to the boiling point, that, for *n*-hexane, is 67 °C. The fact that all the tested gasolines have a behavior very close to that of *n*-hexane would indicate that their saturation temperature at ambient pressure is similar. Moreover, it is clear that in these operating conditions, flash boiling start to affect the spray structure even at low superheating.

A similar behavior is noticed in the whole range of the experimental chamber air pressures explored. When the air pressure is changed, the curve of the near field spray angle bends up at temperature values decreasing with pressure decrease. For all the pressure values, all the gasolines and *n*-hexane show a similar behavior, while *n*-heptane and isooctane can be clearly distinguished from the other fuels. This difference was already observed and emphasized by other researchers [14,16,22], coming to the conclusion that the use of these hydrocarbons as test fluids in flash boiling experiments could lead to wrong indications.

In Fig. 7(a–d) the behavior of the far field spray angle in the range 20–30 mm distance from the nozzle is shown. High angle variations are indicated by the large error bars, however a clear reduction of the angle when the fuel temperature is increased is shown. Therefore, the measurement at different distances from the injector tip can give opposite results in terms of spray angle.

The knowledge of the saturation pressure curve of the pure hydrocarbons (*n*-hexane, *n*-heptane and isooctane), gives an immediate clear view of the link existing between the boiling point at the test air pressure and the flash boiling effects on the spray structure. In fact, as soon as the fuel temperature reaches the boiling value corresponding to the air pressure in the test chamber, an immediate increase of the near field angle of the spray is noticed.

Different characteristic parameters were presented in literature to correlate the behavior of some of the spray characteristics in presence of flash boiling. Typically the superheating degree ($T_f - T_s$), the Jakob number in its form $Ja = (\rho_l/\rho_v)c_p(T_f - T_s)/\Delta H_v$) and the ratio between the saturation pressure and the ambient pressure were used for this scope. This last parameter was presented in literature under different forms: as $\Pi = (p_s - p_a)/p_a$ [4], (p_s/p_a) [9] and (p_a/p_s) [12]. The authors want to underline that the use of these parameters is limited to injectors that in normal conditions work in fully developed breakup regime. As observed by Lamanna et al. [28], in different working conditions these parameters are not controlling the onset of flashing regime.

As already reported in a previous work [9], plotting the near field spray angle in terms of the ratio between the saturation pressure at the experimental temperature and the air pressure (p_s/p_a), all the curves tend to merge.

An example is reported in Fig. 8, where the data obtained for *n*-hexane are reported both in terms of fuel temperature (a) and in terms of (p_s/p_a) (b).

Looking at Fig. 8b an effect of ambient pressure is noticed. As ambient pressure decreases the spray angle curve become slightly steeper, however, for the current purpose, this effect can be considered negligible.

In the present data analysis all the three parameters cited above will be employed and compared for the analysis of the three pure hydrocarbons tested. As it will be shown, all the three parameters permit a good data correlation, merging the curves obtained at different

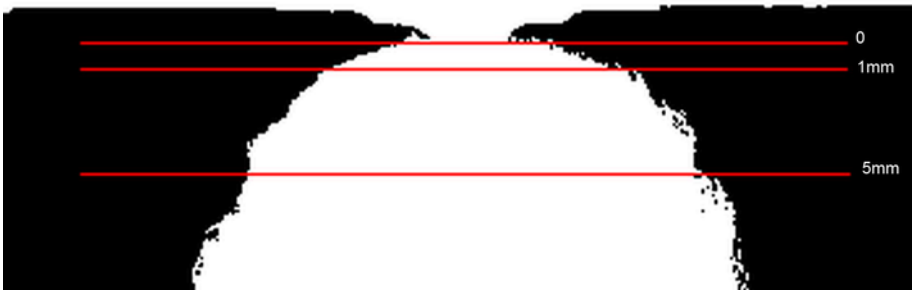

Fig. 4. Binary image of the near field spray in flash boiling conditions.

Table 1
Experimental conditions.

Fuels	*n*-Hexane, *n*-heptane, isooctane, Fuel04, Fuel06, Fuel 08, Fuel95
Injection pressure	10 MPa
Chamber pressure	40 kPa, 60 kPa, 80 kPa, atmospheric
Injector temperature	30, 50, 70, 90, 110 °C

chamber pressures and different fuels in a unique approximated fitting curve. The dispersion of the subcooled angle data makes difficult a precise determination of the beginning of the ascending branch of the curves for the fuels. So a clear comparison of the different fuels in this respect is critical. For the same reason the fitting data range was chosen considering only the data that, from the graphs, clearly appeared as pertaining to the rising part of the curve. The same data range was used for the global fittings shown in the following figures.

In Fig. 9 the near field semiangle of all the pure hydrocarbon fuels employed is reported in terms of superheating degree ($T_f - T_s$). The

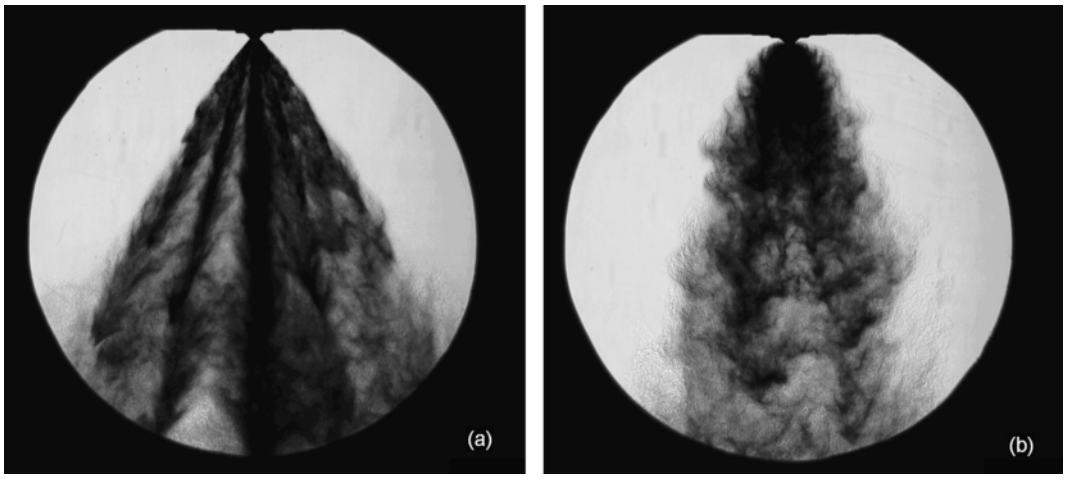

Fig. 5. Images of *n*-hexane spray in absence of flash boiling (a) and in flash boiling conditions (b).

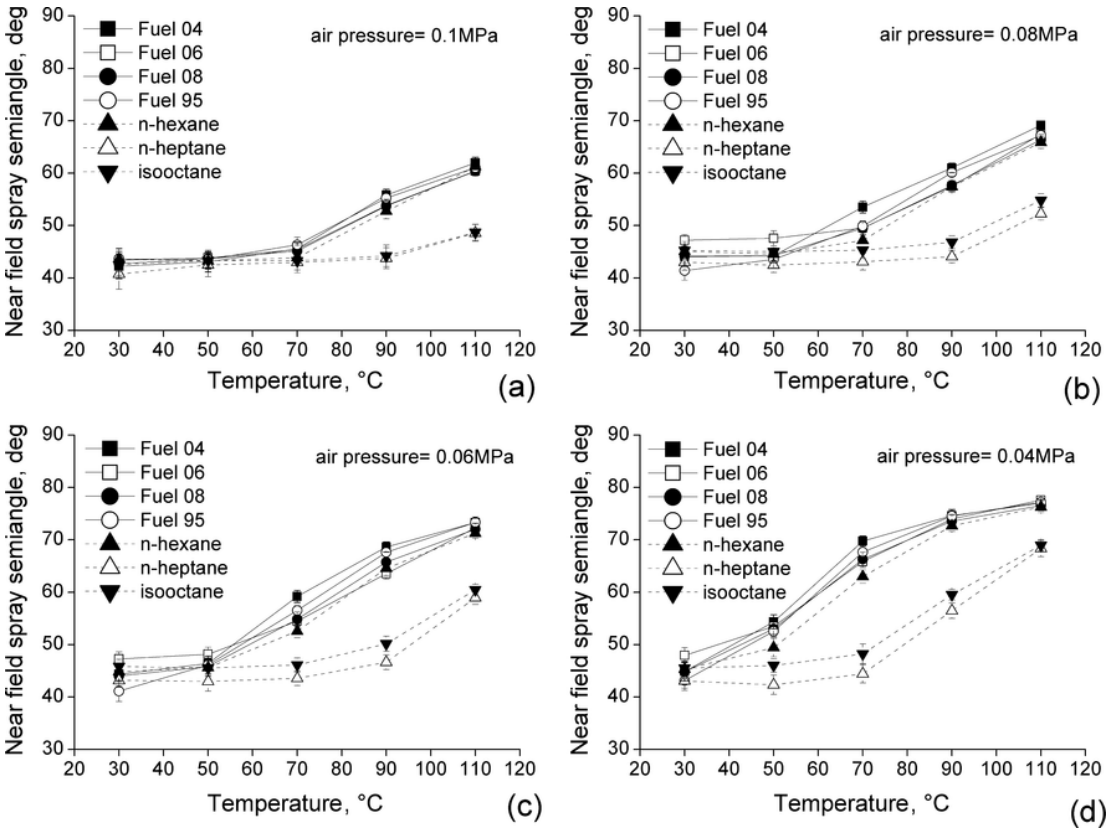

Fig. 6. Near field (0–1 mm) spray semiangles vs. fuel temperature at different chamber pressure: 0.1 MPa (a), 0.08 MPa (b), 0.06 MPa (c), 0.04 MPa (d).

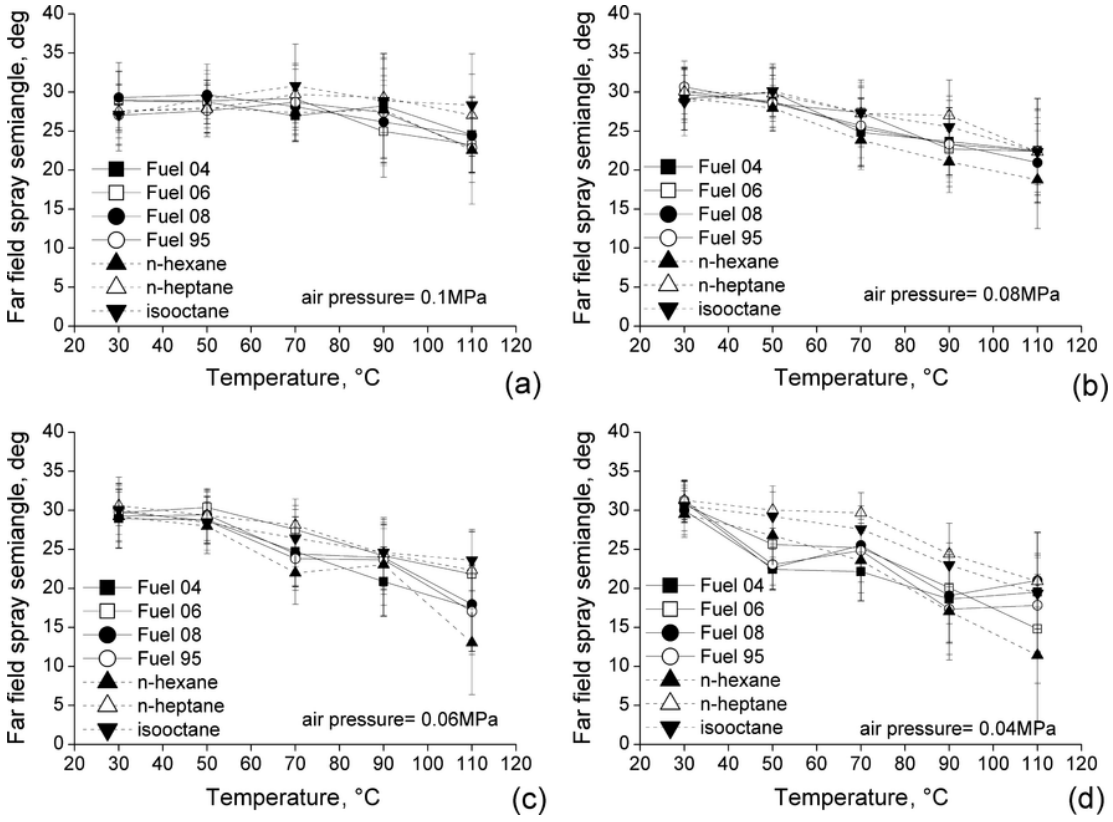

Fig. 7. Far field (20–30 mm) spray semiangles vs. fuel temperature at different chamber pressure: 0.1 MPa (a), 0.08 MPa (b), 0.06 MPa (c), 0.04 MPa (d).

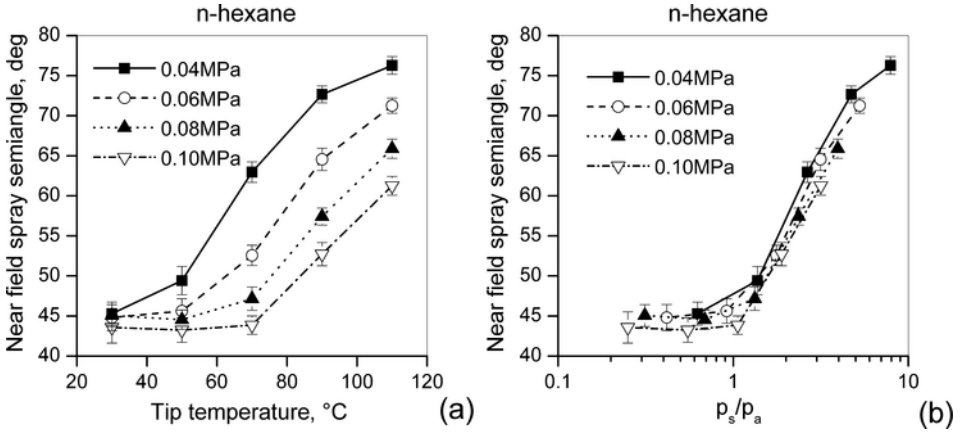

Fig. 8. *n*-Hexane near field spray semiangle at different chamber air pressures in terms of injector tip temperature (a) and in terms of ps/pa (b).

angle starts to increase when $(T_f - Ts) \approx 0$. The data were fitted for $(T_f - Ts) > 5$ °C and the best data fitting is a linear function with $R^2 = 0.89$.

In Fig. 10 the same data are reported in terms of Jakob number. In this case the data were fitted for $Ja > 10$. The best fitting function is logarithmic and its R^2 is 0.95.

In Fig. 11 the correlating parameter is the p_s/p_a ratio. The data were fitted for $p_s/p_a > 1.2$. The best fitting function is logarithmic and its R^2 is 0.93.

All the three correlation parameters are suitable for data reduction. The fitting in terms of p_s/p_a ratio has an R^2 only slightly lower of that obtained with Jakob number. However the parameter p_s/p_a has the advantage of being easier to calculate and it is more physically sound that flash boiling starts to occur at $p_s/p_a \geqslant 1$. For these reasons and for what will be shown later, the p_s/p_a ratio was chosen for the following analysis. It is clear from the figure that the slope for *n*-heptane is higher than that of the other two fuels. In particular the individual slope values are: 19.5 for *n*-heptane, 17.7 for isooctane and 17.9 for *n*-hexane. On the other hand, the average subcooled angle for isooctane is higher than that of *n*-heptane. However, the ±5% bands of the global fitting curve reported in the plot show a good degree of approximation for this way of comparing the data collected in different operating conditions.

As it was shown in the previous figures, the onset of flash boiling causes an increase of the near field spray angle. The opposite effect is shown in Fig. 12 for the far field angle. In this case, when $p_s/p_a > 1$

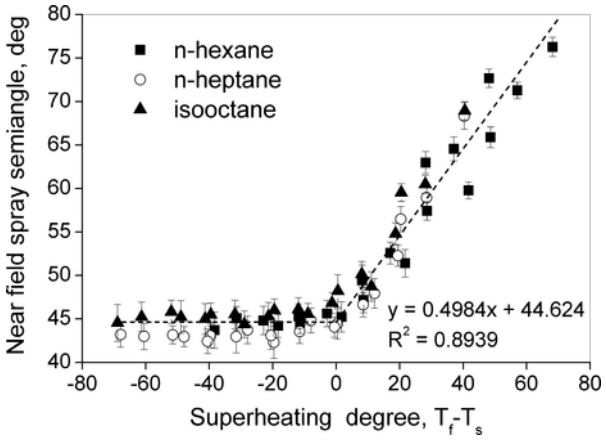

Fig. 9. Near field spray semiangle of the tested pure hydrocarbons in terms of superheating degree ($T_f - T_s$).

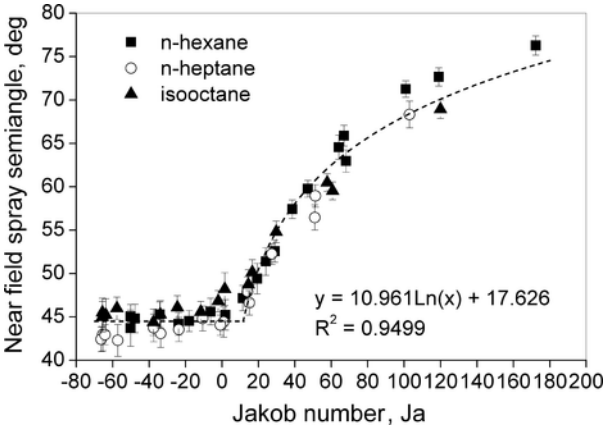

Fig. 10. Near field spray semiangle of the tested pure hydrocarbons in terms of Jakob Number.

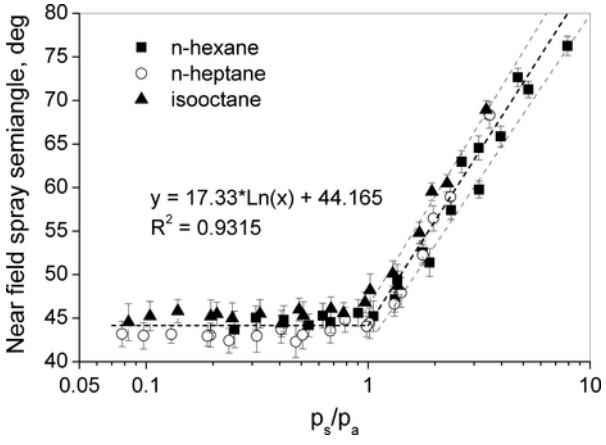

Fig. 11. Near field spray semiangle of the tested pure hydrocarbons in terms of saturation pressure/air pressure ratio ps/pa.

the angle shows a clear decrease. Thus, the expansion of the near field spray angle due to flash boiling has the consequence of contracting the far field spray angle up to the spray collapse. As previously mentioned, this effect is commonly explained by the decrease of the droplet mean diameter, however some other factors influencing the overall induced air flow field could be accounted for. For example, Moon at al. [25] observed clear dissimilar effects between flashing and non flashing conditions, in terms of pressure difference between inner and outer part of the spray of a swirl injector. Even more complex is the case of multihole injectors, where the different spray plumes interact in different ways depending on the injector pattern. It is also to be noticed that the subcooled angle measured in the far field is considerably smaller than that measured in the near field. Obviously, even in subcooled conditions the induced air flow field has the effect of curving the spray side edge toward the axis as the distance from the nozzle increases.

As shown in Figs. 6 and 7 the tested gasolines have a behavior similar to that of *n*-hexane. It is conceivable that the saturation pressure curves of the gasolines are close to that of *n*-hexane and that both the increase of the near field angle and the decrease of the far field angle for the gasolines start at $p_s/p_a = 1$. In the following section an approximated method for the calculation of the saturation pressure curve for a gasoline starting from its distillation curve and its aromatic content will be described.

4. Construction of the saturation pressure curve from the ASTM D86 distillation curve

The data available for the different types of gasoline used in the tests are:

- the ASTM D86 distillation curve,
- the aromatic content.

The distillation curves of the three gasolines used in these tests are presented in Fig. 13.

The volumetric aromatic contents were 30.9% for Fuel04, 34.2% for Fuel06 and 29.2% for Fuel08.

From these data, it was possible to obtain an approximated saturation pressure curve.

The first step was the transformation of the ASTM D86 curve of the gasoline in the corresponding True Boiling Point (TBP) curve. This passage was obtained through the analytical correlation given by Riazi [29]

$$\mathrm{TBP} = a\,(\mathrm{ASTM\ D86})^{b} \tag{1}$$

where the ASTM D86 temperatures are in Kelvin and the constants a and b, at different values of the volume percentage of the distillation curve, are given by Riazi [29].

In Fig. 14, the given ASTM D86 distillation curve and the True Boiling Point calculated curve for one of the gasolines are reported.

From the volume distillation intervals of the TBP curve seven "pseudocomponents" were defined. These pseudocomponents are characterized by the average boiling temperature of the distillation interval and their composition is approximated by a mixture of paraffinic and aromatic hydrocarbons. As the lower boiling aromatic is benzene (80 °C), the pseudocomponents characterized by a lower boiling temperature were considered as composed by paraffines. The other pseudocomponent composition was approximated by a mixture of paraffines and aromatics in a constant proportion to respect the given total aromatic content.

Olsen [30] gives regression curves, calculated from DIPPR data, for molar density in function of the boiling temperature for *n*-paraffins, isoparaffins, cycloalkanes and mono-aromatics. The curves of paraffins and isoparaffins are almost coincident and the curve of cy-

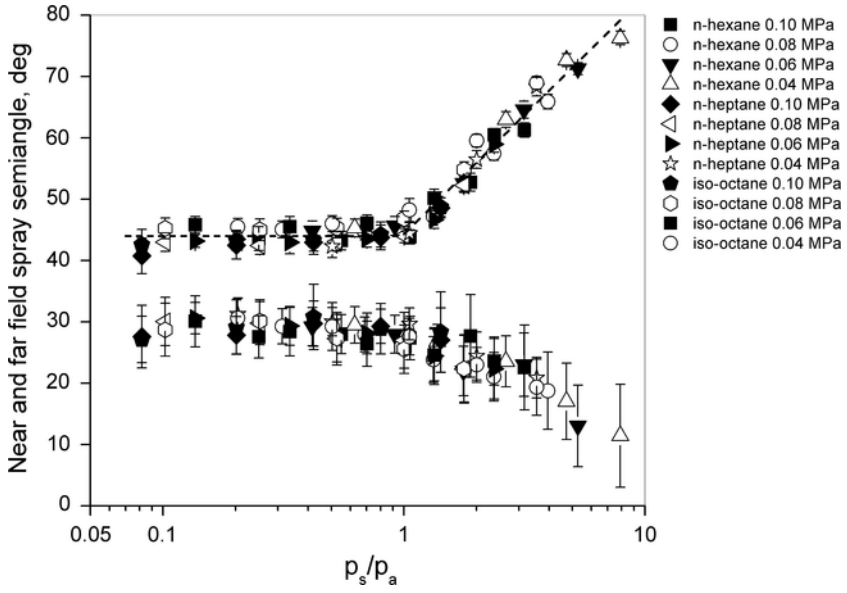

Fig. 12. Near and far field spray semiangles of all the tested pure hydrocarbons in terms of saturation pressure/air pressure ratio ps/pa.

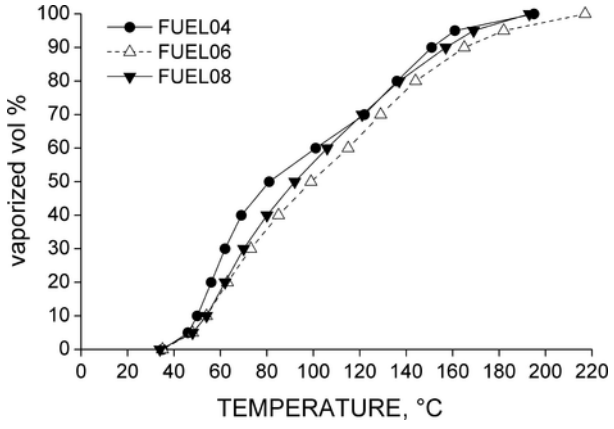

Fig. 13. Distillation curves of the tested gasolines.

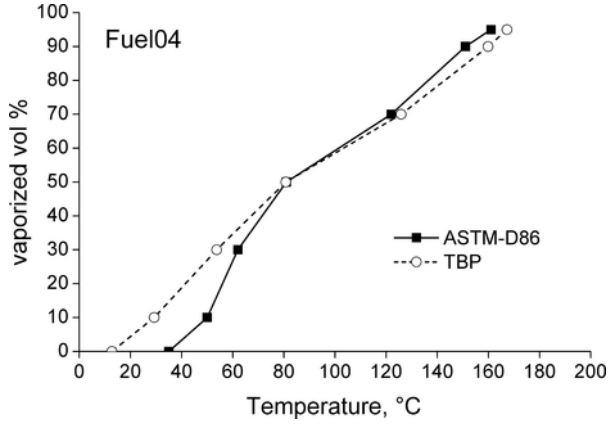

Fig. 14. Fuel 04 ASTM-D86 and calculated True Boiling Point curves.

cloalcanes is approximately an average of the curves of *n*-paraffins and monoaromatics.

The molar volume fraction x_i of each pseudocomponent was than obtained from the average molar density of its paraffinic and aromatic content obtained from Olsen's curves.

Each pseudocomponent saturation pressure p_{si} was then estimated using the model presented by Dutt [31] for pure hydrocarbons.

An Antoine type relationship between vapor pressure and temperature is given:

$$\log(p_{si}) = A - B/(C + T) \tag{2}$$

The constants B and C are given in terms of boiling temperature T_b as:

$$B = m + nT_b \tag{3}$$

$$C = m' + n'T_b \tag{4}$$

the constants A, m, n, m′, n′ are given by Dutt [31] for the different families of hydrocarbons.

The p_{si} value was obtained, in the same way of the molar fraction, by averaging the values of saturation pressure obtained for paraffines and aromatics, according to the given content in the gasoline. The global saturation pressure curve was obtained from the sum over the seven pseudocomponents:

$$p_s(T) = \sum x_i p_{si}(T). \tag{5}$$

The saturation curves obtained with this method are reported together with isooctane, *n*-heptane and *n*-hexane curves in Fig. 15.

These saturation pressure curves, calculated for the three gasolines whose distillation curve was known, permit to plot the near field spray angles in the same way as for the pure hydrocarbons. This is shown in Fig. 16, where the dashed lines reported are the same of Fig. 9. This means that even in this approximated approach the near

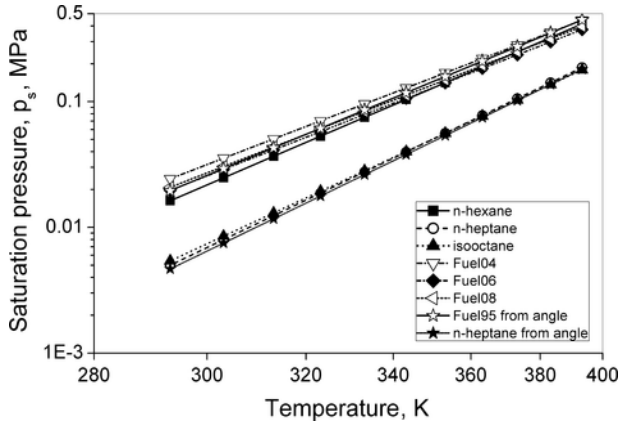

Fig. 15. Saturation pressure curves of the tested fuels (temperature in reciprocal scale).

field angle expansion starts when the (p_s/p_a) ratio is about equal to one.

5. Construction of the saturation pressure curve from experimental near field angle

For Fuel95, whose distillation curve is unknown, it was not possible to apply the same method of data reduction. However, considering valid the behavior observed for the other fuels, it is possible to found, from the experimental data concerning the near field angle variation with fuel temperature (Fig. 17), an approximate saturation curve for this gasoline. Considering the relationship linking the spray angle to p_s/p_a for *n*-hexane valid also for the other fuels, the value of p_s/p_a for Fuel95 can be obtained from the experimental spray angles. In this case the influence of ambient pressure, that was considered negligible for data reduction, is accounted for. Therefore, using the logarithmic fittings of the hexane spray angle data with $p_s/p_a > 1$ at different ambient pressures, it was possible to obtain the p_s/p_a value from the Fuel95 spray angle data obtained at the same air pressure. In Fig. 18 the saturation pressure values deduced from the experimental spray angles of Fuel95 at different air pressure are reported in terms of absolute fuel temperature. These data were fitted obtaining a curve of the type $p_s = \exp(a - b * 1/T)$. As shown in Fig. 15, the saturation pressure curve of Fuel95 obtained with this procedure falls among the other gasoline curves. As the real saturation pressure curve for this gasoline is not available, a direct evaluation of the accuracy of the method for this gasoline is impossible. For this reason, the same procedure was applied to a fuel of known saturation pressure curve. In particular the method was applied to *n*-heptane data. The obtained curve is reported in Fig. 15 and it results to be very close to the one given by NIST [32]. The difference between the real and the reconstructed saturation pressure varies, in the range of interest, from 6% to 3%.

It is obvious that plotting the Fuel95 results in terms of .p_s/p_a using the found $p_s(T)$ curve, the data merge on the same curve of the other fuels.

6. Conclusions

The experimental results of this study show the effects of the increase of fuel temperature on the spray angles of a multi-hole injector operated with three pure hydrocarbons (*n*-hexane, *n*-heptane, and isooctane), three gasolines of known distillation curve and a commercial 95 RON gasoline. The results are mainly focused on the near field angle, measured in the range of 1 mm from the injector tip. For comparison, a far field angle, measured in the range between 20 and 30 mm from the injector tip, was also reported.

A first analysis was performed on the experimental results obtained with pure hydrocarbons to have a reliable data set for a comparison with literature results and with the following analysis based on the results obtained with the different gasolines. Although it is impossible to compare quantitatively the results reported in literature because of the absence of a common procedure for the spray angle measurement under flash boiling conditions, some general trends were confirmed. In particular: the spray angle data obtained at different fuel temperature and different chamber air pressure can be compared in terms of the ratio between saturation pressure at the given fuel temperature and chamber pressure (p_s/p_a). In this way the curves

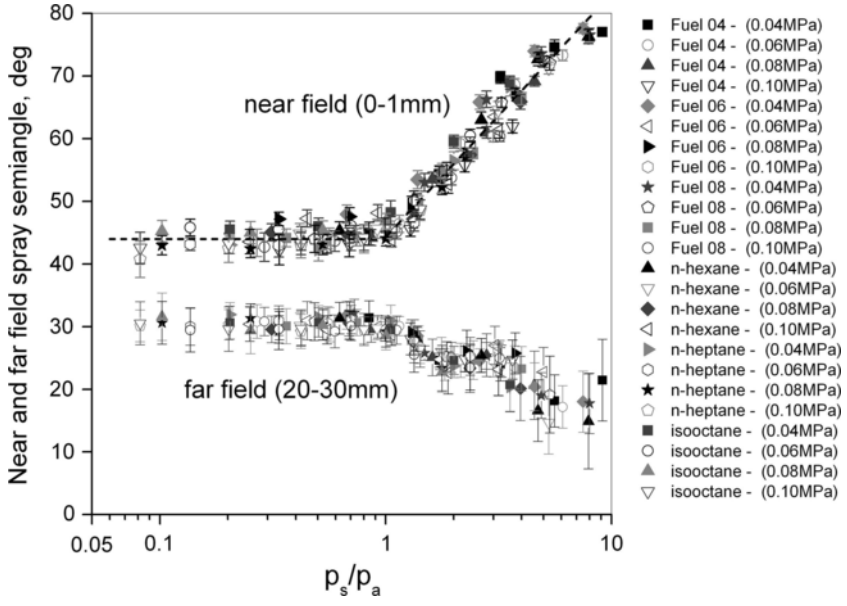

Fig. 16. Near and far field spray semiangle of all the tested fuels in terms of saturation pressure/air pressure ratio ps/pa.

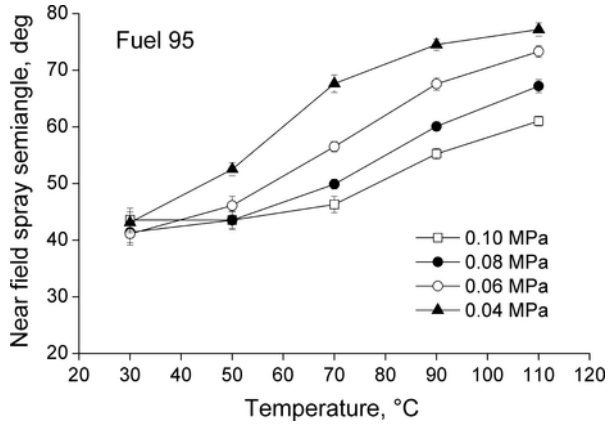

Fig. 17. Fuel95 near field spray semiangle at different chamber air pressures in terms of fuel temperature.

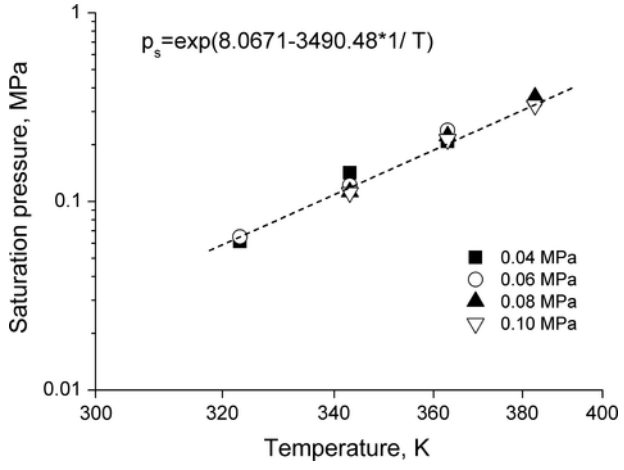

Fig. 18. Saturation pressure curve of Fuel95 calculated from spray semiangle at different chamber pressure.

for the different hydrocarbons at different chamber pressures tend to merge to a unique curve.

To compare in the same way the results obtained for the gasolines, an approximate saturation pressure curve was calculated. Two procedures were presented.

1. Starting from the ASTM D86 distillation curves, it was possible, using correlations reported in literature, to find an approximated saturation curve for each gasoline. From these curves it was possible to plot the gasoline spray angles in terms of p_s/p_a ratio. In this type of plot the gasoline data have the same behavior of the pure hydrocarbon data.
2. As the near field spray angle for a given injector is correlated with p_s/p_a ratio, it is possible to obtain an approximated saturation curve $p_s(T)$ for an unknown composition fuel by comparing its near field spray angle behavior on the same injector with that of a fuel of known $p_s(T)$ curve.

Finally, from the brief literature survey reported in the introduction and the above experimental outcomes, a general conclusion can be draft: a suitable recommended practice for the testing of G-DI fuel injectors in flash boiling conditions is needed.

The spray angle, in flash boiling conditions, has a transition from expanding in the near field to contracting in the far field. Therefore, the most urgent point is a spray angle definition that could give, with a good approximation, an "initial" spray angle avoiding the following transition region. In this way some ambiguous results reported in literature will be avoided. Moreover, as the maximum effect of flash boiling occurs at the nozzle exit, this angle definition will give the maximum sensitivity of the measured angle to the increase of p_s/p_a ratio.

The second point is the choice of *n*-hexane as reference fuel. This choice seems to be generally accepted in laboratories where flash boiling is a consolidated research interest, however in other laboratories either the standard *n*-heptane indicated by the SAE J2715 procedure or isooctane are commonly utilized. Clearly, any pure hydrocarbon can be used as far as the data are normalized with the p_s/p_a ratio. However, since *n*-hexane and gasoline have a similar behavior with respect to flash boiling, the choice of *n*-hexane as reference fuel will simplify testing procedures.

The attempt to obtain an injector independent description of the flash boiling spray in its whole aspect, based on simple correlations and normalizations is quite ambitious. Nevertheless, a common experimental background could facilitate the direct quantitative comparison of the experimental data from different laboratories supplying a vast and reliable database for model validation.

References

[1] R. Brown, J.L. York, Sprays formed by flashing liquid jets, AIChE J 8 (2) (1962) 149–153.

[2] E. Sher, T. Bar-Kohany, A. Rashkovan, Flash-boiling atomization, Prog Energy Combust Sci 34 (2008) 417–439.

[3] B.A. Vanderwege, S. Hochgreb, The effect of fuel volatility on sprays from high-pressure swirl injectors, In: Symposium (international) on combustion, vol. 27, Elsevier, 1998, pp. 1865–1871 (2).

[4] Brad Alan Vanderwege, The effects of fuel volatility and operating conditions on sprays from pressure-swirl fuel injectors, Massachusetts Institute of Technology, 1999. [PhD thesis].

[5] VanDerWege BA, Hochgreb S. Effects of fuel volatility and operating conditions on fuel sprays in DISI engines: (1) imaging investigation. No. 2000-01-0535. SAE technical paper; 2000.

[6] VanDerWege BA, Hochgreb S. Effects of fuel volatility and operating conditions on fuel sprays in DISI engines: (2) PDPA investigation. No. 2000-01-0536. SAE technical paper; 2000.

[7] Araneo L, Coghe A, Brunello G, Dondé R. Effects of fuel temperature and ambient pressure on a GDI swirled injector spray. No. 2000-01-1901. SAE technical paper series; 2000.

[8] Dondé R, Brunello G, Araneo L, Coghe A. Effect of fuel temperature on the mixing properties of a GDI spray, open meeting on combustion. In: 23rd Event of the Italian Section of the Combustion Institute, V. 2; 2000.

[9] L. Araneo, K. Ben Slima, R. Dondé, Flash boiling effect on swirled injector spray angle, In: 18th Annual conference on liquid atomization and spray systems ILASS-Europe, 2002.

[10] S.E. Parrish, R.J. Zink, Spray characteristics of multi-hole injectors under flash boiling conditions, In: 21st Annual conference on liquid atomization and spray systems ILASS – Americas, 2008.

[11] G. Zhang, M. Xu, Y. Zhang, D.L. Hung, Characteristics of flash boiling fuel sprays from three types of injector for spark ignition direct injection (SIDI) engines, In: Proceedings of the FISITA 2012 world automotive congress, Springer, Berlin Heidelberg, 2013, pp. 443–454.

[12] W. Zeng, M. Xu, G. Zhang, Y. Zhang, D.J. Cleary, Atomization and vaporization for flash-boiling multi-hole sprays with alcohol fuels, Fuel 95 (2012) 287–297.

[13] S. Yang, Z. Song, T. Wang, Z. Yao, An experiment study on phenomenon and mechanism of flash boiling spray from a multi-hole gasoline direct injector, Atom Sprays 23 (5) (2013) 379–399.

[14] Schmitz I, Leipertz A. Comparison of the flash boiling influence on the spray structure of a high pressure swirl injector and of a multihole injector for GDI engines – 10th international conference on liquid atomization and spray systems paper ID ICLASS06-026; 2006.

[15] Heldmann M, Knorsch T, Schmitz I, Wensing M, Leipertz A. Investigation of significant spray rotation phenomena under flash-boiling conditions studied on a multi-hole DISI injector for bio-ethanol E85 and gasoline E5. In: 24th Annual conference on liquid atomization and spray systems ILASS – Europe); 2011.

[16] Weber D, Leick P. Structure and velocity field of individual plumes of flashing gasoline direct injection sprays. In: 26th Annual conference on liquid atomization and spray systems, ILASS – Europe; 2014.

[17] M. Mojtabi, G. Wigley, J. Helie, The effect of flash boiling on the atomization performance of gasoline direct injection multistream injectors, Atom Sprays 24 (6) (2014) 467–493.
[18] Mojtabi M, Chadwick N, Wigley G, Helie J. The effect of flash boiling on breakup and atomisation in GDI sprays. In: Proceedings of the 22nd European conference on liquid atomization and spray systems. paper ID ILASS08-6-1; 2008.
[19] Allocca L, Montanaro A, Di Gioia R, Bonandrini G. Spray characterization of a single-hole gasoline injector under flash boiling conditions No. 2014-32-0041. SAE technical paper; 2014.
[20] J. Serras-Pereira, Z. Van Romunde, P.G. Aleiferis, D. Richardson, S. Wallace, R.F. Cracknell, Cavitation, primary break-up and flash boiling of gasoline, iso-octane and n-pentane with a real-size optical direct-injection nozzle, Fuel 89 (9) (2010) 2592–2607.
[21] P.G. Aleiferis, Z.R. Van Romunde, An analysis of spray development with iso-octane, n-pentane, gasoline, ethanol and n-butanol from a multi-hole injector under hot fuel conditions, Fuel 105 (2013) 143–168.
[22] P.G. Aleiferis, J. Serras-Pereira, A. Augoye, T.J. Davies, R.F. Cracknell, D. Richardson, Effect of fuel temperature on in-nozzle cavitation and spray formation of liquid hydrocarbons and alcohols from a real-size optical injector for direct injection spark-ignition engines, Int J Heat Mass Transf 53 (2010) 4588–4606.
[23] Matsumoto A, Xie X, Zheng Y, Lai MC, Moore W. Direct injection multi-hole spray and mixing characterization of ethanol gasoline blends in engine. In: 22nd Annual conference on liquid atomization and spray system, ILASS Americas; 2010.
[24] Postrioti L, Bosi M, Cavicchi A, AbuZahra F, Di Gioia R, Bonandrini G. Momentum flux measurement on single-hole GDI injector under flash-boiling condition No. 2015-24-2480. SAE technical paper; 2015.
[25] S. Moon, C. Bae, E.F. Abo-Serie, J. Choi, Internal and near-nozzle flow of a pressure-swirl atomizer under varied fuel temperature, Atom Sprays 17 (6) (2007) 529–550.
[26] D.L. Hung, D.L. Harrington, A.H. Gandhi, L.E. Markle, S.E. Parrish, J.S. Shakal, et al., Gasoline fuel injector spray measurement and characterization-a new SAE J2715 recommended practice, SAE Int J Fuels Lubr 1 (2008-01-1068) (2008) 534–548.
[27] Gary S. Settles, Schlieren and shadowgraph techniques: visualizing phenomena in transparent media, Springer Science & Business Media, 201242.
[28] G. Lamanna, H. Kamoun, B. Weigand, J. Steelant, Towards a unified treatment of fully flashing sprays, Int J Multiph Flow 58 (2014) 168–184.
[29] Riazi MR. Characterization and properties of petroleum fractions. ASTM; 2005.
[30] E. Olsen, Method to calculate the vapour pressure of hydrocarbon solvents from simple physic-chemical properties, National Institute of Occupational Health, Copenhagen, 2003. http://www.esig.org/uploads/ModuleXtender/Publications/141/91-660-vp_paper_olsen_june_2003-1-.pdf.
[31] N.V.K. Dutt, Estimation of vapor pressure from normal boiling point of hydrocarbons, Region Res Lab, Canad J Chem Eng 60 (5) (1982) 707–709.
[32] Linstrom PJ, Mallard WG, editors. NIST chemistry webbook, NIST standard reference database number 69, National Institute of Standards and Technology, Gaithersburg MD, 20899. <http://webbook.nist.gov>.